Short Communication:

Synthesis, Characterization, and Antioxidant Activity of Cr(III), Mn(II), Fe(III), Co(II) and Ni(II) Complexes with Mixed Azo Dye and Bipyridyl Ligands

Areej Kamal Assim Aldabbagh[1*], Mawlood Khalid Mawlood[2], and Abbas Ali Salih Al-Hamdani[1]

[1]Department of Chemistry, College of Science for Women, University of Baghdad, Baghdad 10071, Iraq

[2]Department of Chemistry, College of Education, University of Samarra, Saleh Aden 34010, Iraq

Abstract: *Mixed ligands reaction of [2-[(3-hydroxyphenyl)diazinyl]-1,2-benzothiazol-3(2H)-one-1,1-dioxide] (H₂L, primary ligand) and bipyridyl (secondary ligand) with salts of Cr(III), Mn(II), Fe(III), Co(II) and Ni(II) was performed. A series of air-stable complexes with distinctive octahedral moieties was created by equal molar ratio (1:1:1). The formation of these compounds was verified using detecting analysis techniques incorporating mass spectra, which validated the achieved geometries. Fourier transform infrared (FTIR) analysis demonstrated how the ligands (H₂L and bipyridyl) are chelated as tridentate (ONO) and bidentate (NN) groups, respectively and the coordination with the metal ions. Thermal decomposition studies using pyrolysis (TGA and DSC) verified that water residues could be coordinated with metal complexes. Additionally, elemental micro-analysis, chlorine amount test, molar conductivity and melting points examination were carried out. Magnetic sensitivity of the susceptibility and ultraviolet-visible (UV-vis) spectrophotometry can also reveal the coordination existence with the metals and complexes formation. The compounds' antioxidant records were finally evaluated using the 1,1-diphenyl-2-picrylhydrazyl (DPPH) radical as a free radical method. It was compared to that of gallic acid as an accordingly standard antioxidant substance with its IC₅₀ value. These complexes could restrict free radicals; [Fe(L)(bipy)Cl] has the best antioxidant activity, whereas [Ni(L)(bipy)H₂O] has the lowest.*

Keywords: *antioxidant values; mass spectra; mixed-ligand complexes; bipyridyl; thermal analysis*

■ INTRODUCTION

One of chemistry's main subjects is the synthesis of new compounds. Mixed ligand complexes occupied a large space in the field of coordination chemistry and other areas, specifically in medicine, industry and agriculture. Multi-topic bridging ligands with two or more functional groups involving nitrogen and/or oxygen are currently well-known to exhibit varying binding capacities to a range of transition metal cations [1-2]. The perspective of these self-assembled coordination models has been emphasized by their use in drug administration, molecular recognition, and catalysis [3]. Studies have also shown the importance of bipyridyl, mostly in the medicine section [4-5]. A significant family of chemical compounds that has

received comprehensive attention lately is titled azo compounds [6-7]. Their function represented by N=N group used as tissue colorants and indicators in analytical chemistry owed to its strong color within the visible region and sensitivity to changes in acidity (pH) [8]. Complexes of binary ions of cobalt, nickel, copper and zinc were prepared with Schiff base 3,2-dimethyl-1-phenyl-4-silidine-3-pyrozoline-5-one (H₂L) as it forms octahedral ionic complexes, in which the ligand behaves as a tridentate chelate [9]. Assemblies as well prepared from mixed ligands of 8-hydroxydimethyl-1-phenyl-4-sylcylidene-3-pyrrozoline-5-one (LH) with manganese, iron, cobalt, nickel and copper ions were formed neutral tetrahedral complexes in it links such as a bidentate

608

Indones. J. Chem., 2025, 25 (2), 607 - 618

chelate [10-11]. Antioxidants may be found in both natural and synthetic sources, and they are essential for boosting immunity throughout the body. The DPPH radical has been used to assess a compound's antioxidant activity by testing its capacity to donate hydrogen or scavenge free radicals by contrasting with those of gallic acid (Ga), the positive control [12].

This research included the synthesis of new complexes from the reaction of Cr(III), Mn(II), Fe(III), Co(II) and Ni(II) salts with bipyridyl (bipy) and azo dye ligand (H_2L), which were characterized. Complexes were identified and studied using the ultraviolet-visible spectrum and infrared, and the metal ratio in complexes by chlorine content determination and measurement of molar conductivity, in addition to measurements of magnetism and melting points. These substances' antioxidant activity was evaluated against the DPPH radical and contrasted with Ga, a naturally occurring antioxidant reference.

■ EXPERIMENTAL SECTION

Materials

All components, chemicals and reagents, were provided from the trading suppliers: Sigma, Merck and used upon receipt, these include inorganic salts: $CrCl_3 \cdot 6H_2O$, $MnCl_2 \cdot 4H_2O$, $FeCl_3$, $CoCl_2 \cdot 6H_2O$, $NiCl_2 \cdot 6H_2O$ (99%), bipy and H_2L [13]. Solvents such as pure ethanol (EtOH) and dimethyl sulfoxide (DMSO) were used as supplied from Aldrich.

Instrumentation

The single-V.3.O-single Euro vector model EA/3000 has been utilized to achieve C.H.N. analysis. Metal ions were calculated as chloride using a gravimetric approach. The molar conductivity of the complexes was measured with a conductometer W.T.W at room temperature in 1×10^{-3} M (DMSO). Mass spectra (MS) QP50A: DI Analysis Shimadzu QP-2010-Plus (E170Ev), electron impact (30 eV) spectrometer was logged for the complexes. The UV-vis absorption spectra to the 200–1100 nm range were obtained using the UV-1800 Shimadzu

spectrophotometer, 10^{-3} M solutions in DMSO at room temperature. For thermogravimetric analysis, studies were carried out using the Perkin-Elmer Pyris Diamond TGA-DSC and the Fourier transform was examined using the IR Prestige-21 to study FTIR spectra. Metals were identified using a Shimadzu (F.A.A) 680 G atomic clock.

Procedure

Preparation of metal complexes

The metal ions complexes for Cr(III), Mn(II), Fe(III), Co(II) and Ni(II) were prepared using metal chlorides (M:L:L=1:1:1). As a stoichiometric amount of $CrCl_3 \cdot 6H_2O$ (1.004 g, 1 mmol), $MnCl_2 \cdot 4H_2O$ (0.612 g, 1 mmol), $FeCl_3$ (0.897 g, 1 mmol), $CoCl_2 \cdot 6H_2O$ (0.896 g, 1 mmol), and $NiCl_2 \cdot 6H_2O$ (0.746 g, 1 mmol) salts dissolved in 20 mL distilled water was gradually added dropwise additions in round bottom flask. An amount of azo ligand (1 g, 0.00377 mol), dissolved in 10 mL pure ethanol, was continually stirred. Then, a bipy substance (0.588 g, 0.00377 mol) was dissolved in 10 mL pure ethanol with stirring. The combination was brought to between 60 and 70 °C for 2 h reverse escalation, cooled in an ice bath until precipitation started to form with color changing, and then permitted to stand for over 6 h. To get rid of any unreacted components, the solid complexes were separated and washed with a small amount of hot-diluted ethanol. A vacuum desiccator was then used to dry the compounds (when varied precipitate colors were gained) with a production rate of 68%. The complexes fragment at the range between 210–240 °C. Scheme 1 shows how the metal ions complexes are created. The ligand and its metal complexes' analytic and physical characteristics are included in Table 1.

■ RESULTS AND DISCUSSION

The elemental analysis of generated metal complexes yielded firm results that were reasonably consistent with theoretical predictions. Elemental investigations revealed that complexes' metal:ligand:ligand ratios were 1:1:1. The physical and analytical details of the azo ligand and their metal complexes are listed in Table 1.
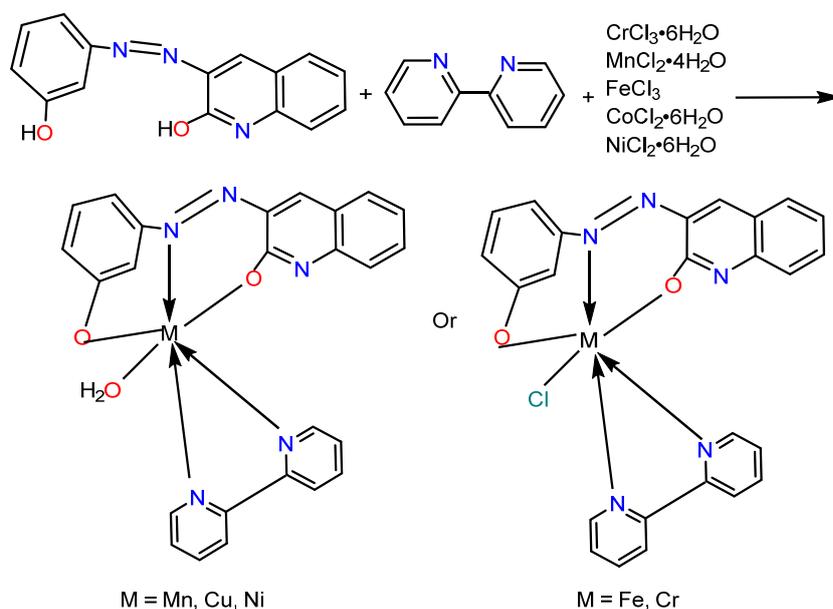
Scheme 1. Synthesized and suggested structures for complexes according to diagnostic results

Table 1. Physical properties and analytical data for the synthesized complexes

Compound	Chemical formula (M.wt)	Color	m.p (°C)	Yield (%)	Elemental microanalysis (%)				
					C(E.)	H(E.)	N(E.)	M(E.)	Cl(E.)
					C(C.)	H(C.)	N(C.)	M(C.)	Cl(C.)
[Cr(L)(bipy)Cl]	$C_{25}H_{17}N_5O_2CrCl$ (506.88)	Brown	210–212d	55	58.69	3.01	14.83	11.05	7.05
					59.24	3.38	13.82	10.26	6.99
[Fe(L)(bipy)Cl]	$C_{25}H_{17}N_5O_2FeCl$ (510.73)	Red brown	238–240d	48	57.91	4.11	14.69	11.48	7.21
					58.79	3.35	13.71	10.93	6.94
[Mn(L)(bipy)H$_2$O]	$C_{25}H_{19}N_5O_3Mn$ (492.39)	Light brown	226–228d	60	60.08	4.01	14.94	11.09	-
					60.98	3.89	14.22	11.16	-
[Co(L)(bipy)H$_2$O]	$C_{25}H_{19}N_5O_3Co$ (496.38)	Brown	218–220d	61	61.22	3.02	15.18	11.16	-
					60.49	3.86	14.11	11.87	-
[Ni(L)(bipy)H$_2$O]	$C_{25}H_{19}N_5O_3Ni$ (496.14)	Red brown	234–236d	40	60.87	2.94	15.17	12.34	-
					60.52	3.86	14.12	11.83	-

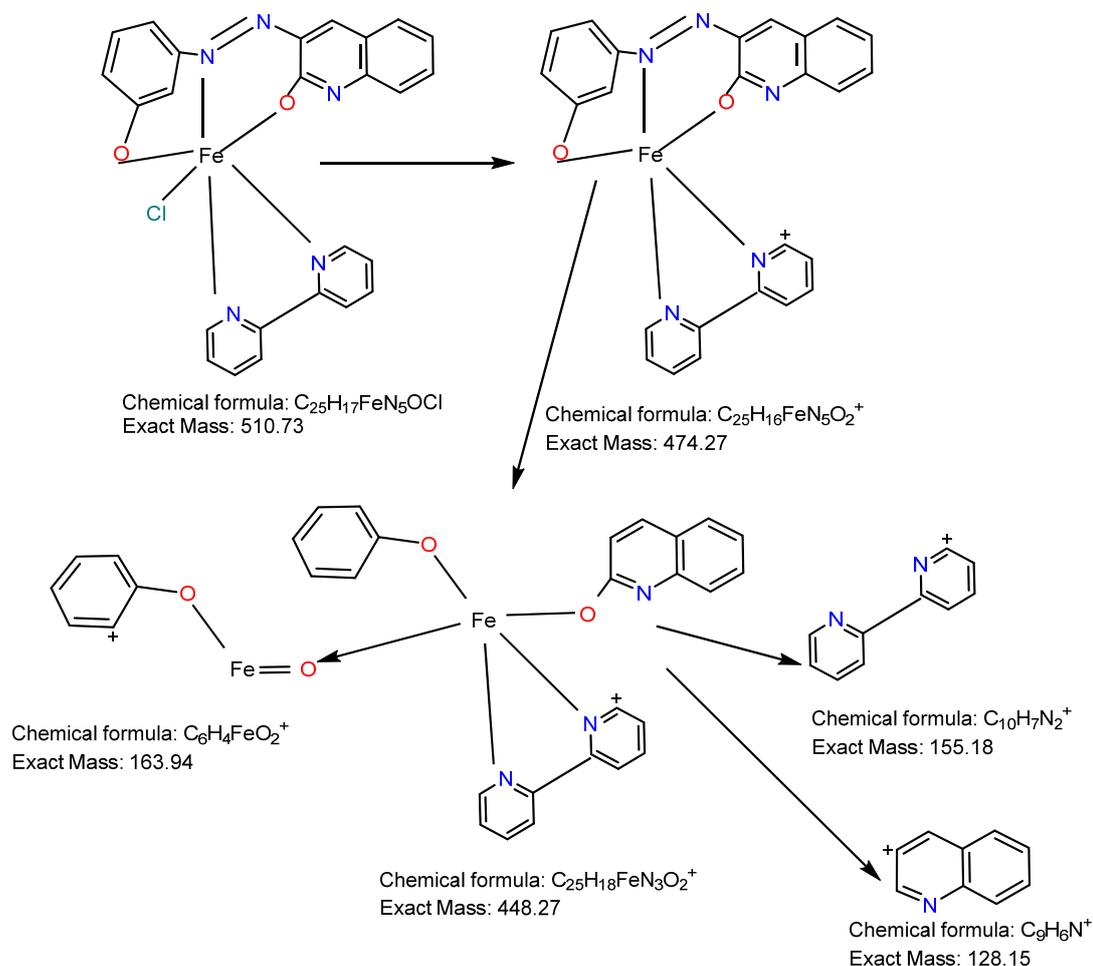E: Experimental, C: Calculated, d means it has reached the point of disintegration

Mass Spectrum

Fig. S1 displays the mass spectra of [Fe(L)(bipy)Cl] and Scheme 2 summarizes the fragmentation pattern at m/z = 510.73. The molecular ion peak reached its highest point, corresponding to the ligand's molecular weight. Further peaks at m/z = 474.27, 448.27, 163.94, 155.18, and 128.15 may be associated with $C_{25}H_{16}FeN_5O_2^+$, $C_{25}H_{18}FeN_3O_2^+$, $C_6H_4FeO_2^+$, $C_{10}H_7N_2^+$, and $C_9H_6N^+$, correspondingly. Fig. S2 displays the mass spectra of [Mn(L)(bipy)H$_2$O] and Scheme 3 summarizes the

fragmentation pattern. The peak of the molecular ion, corresponding to the weight of the ligand, peaked at m/z = 492.39 and exhibits several peaks at m/z = 473.37, 381.27, 354.26, 225.11, and 128.15. These peaks' patterns can be linked to different fragments with the following codes: $C_{25}H_{16}MnN_5O_2^+$, $C_{19}H_{12}MnN_5O^+$, $C_{19}H_{13}MnN_3O^+$, $C_{10}H_6MnN_2O^+$, and $C_9H_6N^+$, respectively [14-15].

Infrared Spectra

The complexes were identified using infrared spectra, and the spectra were then compared to those of

Chemical formula: $C_{25}H_{17}FeN_5OCl$
Exact Mass: 510.73

Chemical formula: $C_{25}H_{16}FeN_5O_2{}^+$
Exact Mass: 474.27

Chemical formula: $C_6H_4FeO_2{}^+$
Exact Mass: 163.94

Chemical formula: $C_{25}H_{18}FeN_3O_2{}^+$
Exact Mass: 448.27

Chemical formula: $C_{10}H_7N_2{}^+$
Exact Mass: 155.18

Chemical formula: $C_9H_6N^+$
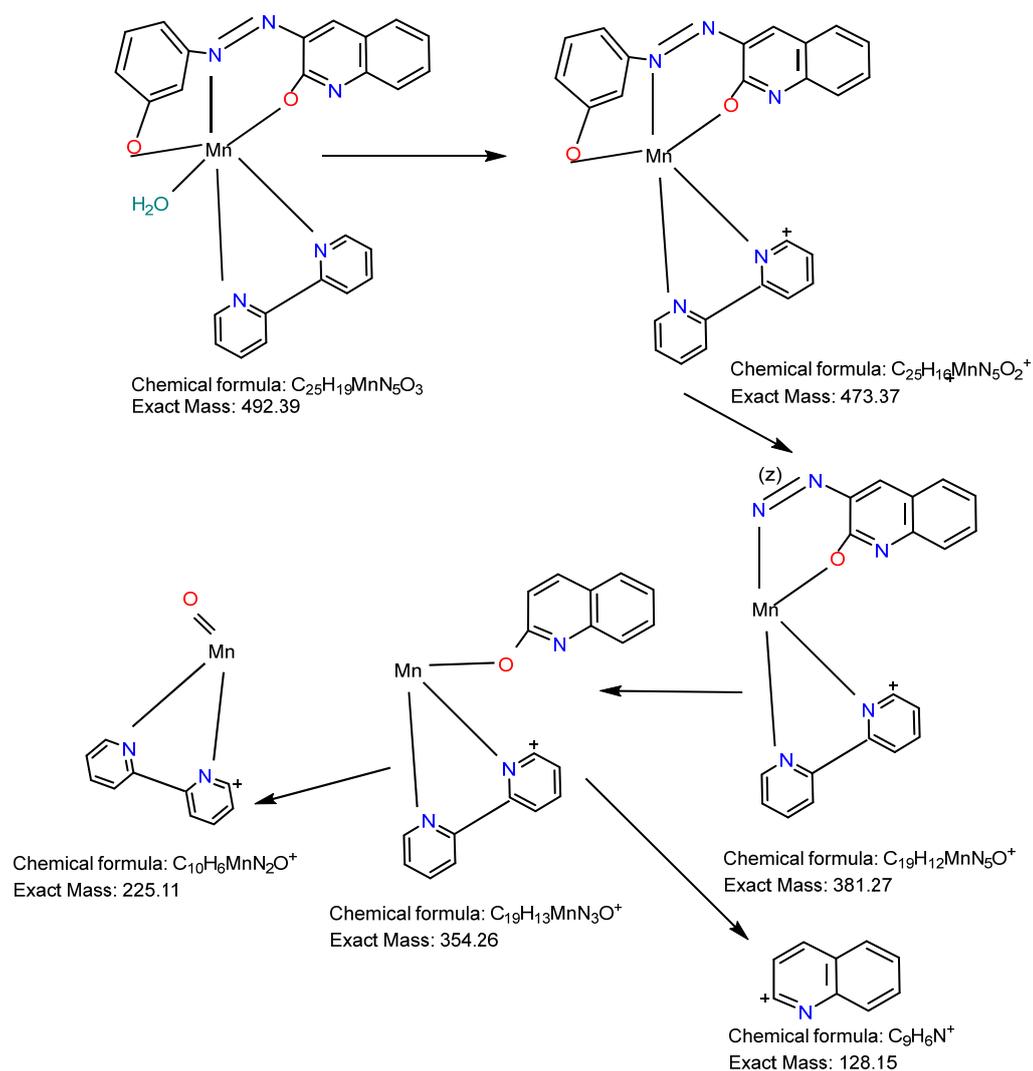Exact Mass: 128.15

Scheme 2. Fragmentation pattern of Fe-complex

the ligands in their free state. Table 2 displays the results of a thorough analysis of the infrared spectra of the produced complexes. The spectra data demonstrate the movement of some bands towards longer or shorter wavelengths, changes in their forms and intensities, the elimination of bands and the creation of new bands for both ligands. A clear shift to a higher wavenumber was observed for the $\nu(N=N)$ band, and this is evidence of a coordination process between the metals and the N–N group. This is confirmed by the appearance of a new band belonging to M–N, as shown in Table 2, in addition to the disappearance of bands belonging to the O–H phenol present in the ligand in the free state. This is evidence of coordination between the phenol group's metals and nitrogen atom, as shown in Table 2. In addition to the appearance of three distinct bands for each manganese,

cobalt and nickel complexes, as shown in Figs. S3 and S4, this is due to the presence of a water molecule. It was also observed that the C=N ring band of the bipy compound in the complexes was shifted from what it was in the free state, as shown in Table 2, there is an absorption band at 1581 cm^{-1}. This is evidence of consistency. The new M–N bands that appeared support these proposed shapes of the complexes. The FTIR spectrum of H_2L shows band at 3465 cm^{-1} returns to $\nu(O–H)$, and bands appeared at 1656 and 1600 cm^{-1} belong to the stretching frequencies $\nu(C=O)$ and $\nu(C=N)$ for azomethane, respectively [16-17].

Electronic Spectral and Magnetic Moments

The molar conductance of ligand complexes, soluble in DMSO solvent in 10^{-3} M solution at 25 °C, characterizes the complexes as non-electrolytic.

Chemical formula: $C_{25}H_{19}MnN_5O_3$
Exact Mass: 492.39

Chemical formula: $C_{25}H_{16}MnN_5O_2{}^+$
Exact Mass: 473.37

(z)

Chemical formula: $C_{19}H_{12}MnN_5O^+$
Exact Mass: 381.27

Chemical formula: $C_{10}H_6MnN_2O^+$
Exact Mass: 225.11

Chemical formula: $C_{19}H_{13}MnN_3O^+$
Exact Mass: 354.26

Chemical formula: $C_9H_6N^+$
Exact Mass: 128.15

Scheme 3. Fragmentation pattern of Mn-complex

Table 2. The locations of the distinct bands of ligands and their metal complexes in the FTIR spectrum (cm^{-1})

Comp.	ν(C–H) aromatic	ν(C=N) aromatic	ν(N=N)	ν(M–N)	ν(M–O)	ν(H_2O) aqua
Ligand H_2L	3167		1325	-	-	-
Bipy	-	1581	-	-	-	-
[Cr(L)(bipy)Cl]	3180	1600	1412	573	530	-
[Fe(L)(bipy)Cl]	3149	1594	1413	569	487	-
[Mn(L)(bipy)H_2O]	3157	1591	1421	573	509	3392
						1640
						824
[Co(L)(bipy)H_2O]	3182	1604	1415	503	461	3421
						1645
						835
[Ni(L)(bipy)H_2O]	3165	1597	1409	589	541	3388
						1642
						828

UV-vis Spectra and Magnetic Susceptibility

The bipy spectrum has absorption bands at 285 and 240 nm. The first band of transmission represents the $\pi \to \pi^*$ electronic transfer, and the second band represents the $n \to \pi^*$ electronic transfer. H_2L electronic spectra show a significant absorption peak at 278 nm, assigned to the $\pi \to \pi^*$ transition and a high-intensity band generated with absorption maxima at 355 nm, due to the $n \to \pi^*$ transition. Transmission-dependent bands ($n \to \pi^*$) are displaced in the ligand towards different wavelengths in its contact with the metal ion, and this displacement is due to the donation of an electron pair from the nitrogen atom of the ligand to the metal ion (M–N). The Cr^{3+} complex's electronic transition shows a peak at 326, 537, 719, and 798 nm that is attributed to $\pi \to \pi^*$, $n \to \pi^*$, ${}^4A2g \to {}^4T1g_{(P)}$, ${}^4A2g \to {}^4T1g_{(F)}$, and ${}^4A2g \to {}^4T2g_{(F)}$, correspondingly. The first peak belongs to the ligand transitions themselves and has been displaced from what they were in the free state, while the remaining peaks belong to the transitions of the metal itself, and their frequency is shown in Fig. S5. It also gave magnetic sensitivity ($\mu_{eff} = 3.771$ B.M), indicating the presence of 3 individual electrons in a paramagnetic capacity, with d^2sp^3 hybridization and an electronic distribution $T_2g^3eg^0$, indicating an octahedral geometry. The Ni^{2+} complex exhibits an electronic transition with a peak at 291, 368, 719, 763, and 821 nm corresponding to $\pi \to \pi^*$, $n \to \pi^*$ + C.T, ${}^3A1g \to {}^3T2g_{(F)}$, ${}^3A1g \to {}^3T1g_{(F)}$, and ${}^3A2g \to {}^3T1g_{(P)}$, respectively. The first peak belongs to the ligand transitions themselves and has been displaced from what they were in the Free State, while the remaining peaks belong to the transitions of the metal itself, and their frequency is shown in Fig. S6. The μ_{eff} value of 2.21 B.M indicates the presence of 3 individual electrons in a paramagnetic capacity (d^2sp^3 hybridization), with an electronic distribution $T_2g^6eg^2$ and an octahedral shape. The Fe^{3+} complex's electronic transition shows a peak at 394, 321, 617, and 634 nm that is attributed to $\pi \to \pi^*$, $n \to \pi^*$ + C.T, ${}^6A_1g \to {}^4Eg_{(G)}$, and ${}^6A1g \to {}^4T2g_{(G)}$, respectively. The first peak belongs to the ligand transitions themselves, which have been displaced from what they were in the free state. In contrast, the remaining peaks belong to the transitions of the metal itself. Their frequency is shown in Fig. S7, with $\mu_{eff} = 5.69$ B.M, suggesting the presence of 3 individual electrons in a paramagnetic capacity (d^2sp^3 hybridization), with an electronic distribution $T_2g^3eg^2$ and an octahedral shape. The Mn^{2+} complex has an octahedral geometry, as indicated by the peak of 268, 433, 462, and 491 nm that is attributed to $\pi \to \pi^*$, ${}^6A1g \to {}^4Eg_{(G)}$, ${}^6A1g \to {}^4T2g_{(G)}$, and ${}^6A1g \to {}^4T1g_{(G)}$, respectively. The first peak belongs to the ligand transitions themselves, which have been displaced from what they were in the free state. In contrast, the remaining peaks belong to the transitions of the metal itself. Their frequency is shown in Fig. S8, with $\mu_{eff} = 5.17$ B.M indicates the presence of 3 individual electrons in a paramagnetic capacity, with d^2sp^3 hybridization, and with an electronic distribution $T_2g^3eg^2$ during its electronic transition. Octahedral geometry is indicated by the electronic spectra of the Co^{2+} molecule, which was investigated. It showed a peak at 287, 338, 617, and 679 nm that was assigned to $\pi \to \pi^*$, $n \to \pi^*$, ${}^4T1gF \to {}^4T1g_{(P)}$, and ${}^4T1gF \to {}^4A1g_{(F)}$ correspondingly, the first peak belongs to the ligand transitions themselves and has been displaced from what they were in the free state, while the remaining peaks belong to the transitions of the metal itself, and their frequency is shown in Fig. S9, with $\mu_{eff} = 3.88$ B.M suggesting the presence of 3 individual electrons, in a paramagnetic capacity, with d^2sp^3 hybridization [18-19], and with an electronic distribution $T_2g^6eg^1$. Table 3 explains the locations of absorption bands for ligands and their complexes.
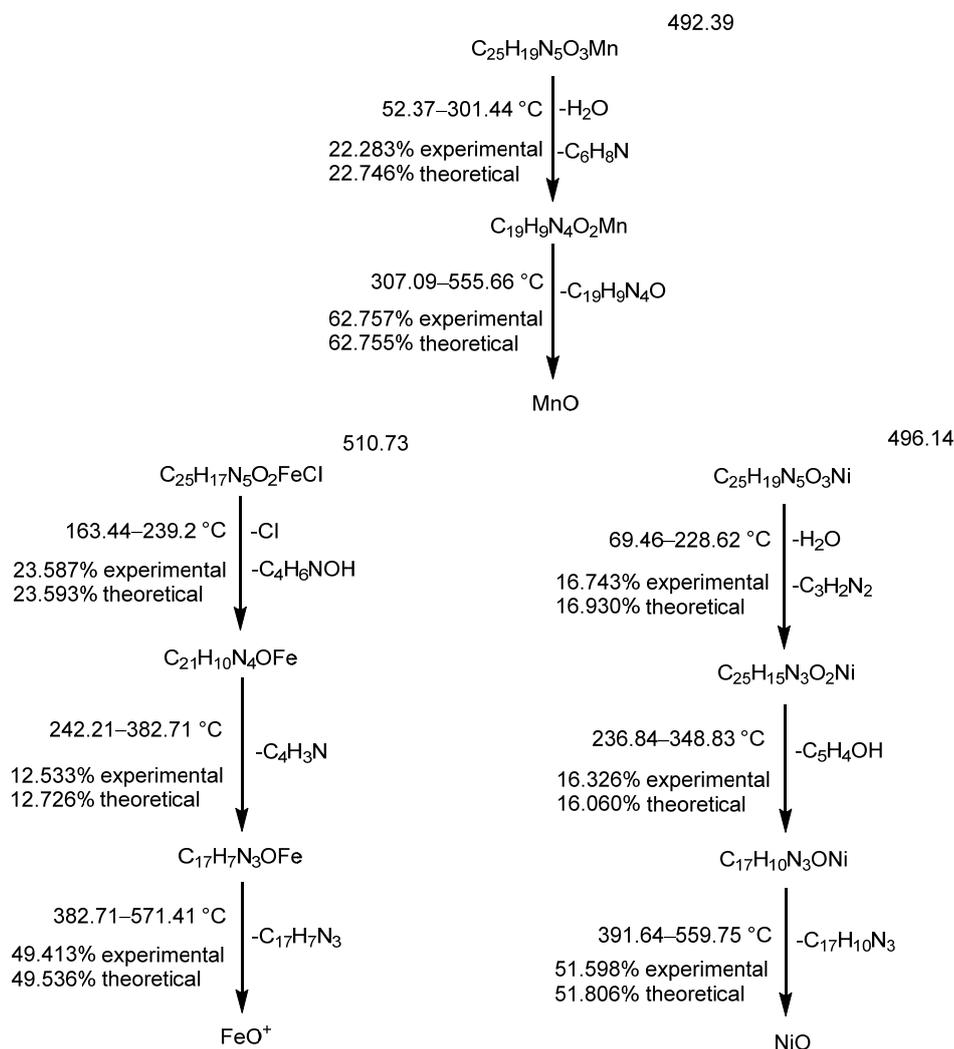
Thermal Measure Readings

Table 4. and Fig. S10–S12 presents the results of the thermal analysis for the synthesized complexes. The possible breakdown reaction of metal complexes is shown in Scheme 4. The weight loss complex percentages, temperature ranges, breakdown products, and phases of decomposition computations showed consistency based on the thermograms. This confirms the elemental analysis results and the suggested equations relating the computed values to their thermal decomposition outcomes. This work gave the results of the thermogravimetric decomposition of complexes Mn^{2+}, Fe^{3+} and Ni^{2+} stages of decomposition. It was observed that the decomposition of the manganese complex included two stages; the first

Table 3. Electronic spectral data (ultraviolet and visible) for ligands in their free state and complexes and molar conductivity in DMSO (1×10^{-3} M) and magnetic susceptibility values

Comp.	λ_{max} (nm)	ν cm^{-1}	Absorption ABS	ε_{max} (L.mol^{-1}.cm^{-1})	Assignment and its type	$\Lambda_m$cm^2 (Ω^-1.mol^{-1})	μ_{eff} B.M	Hybridization	Distribution
H$_2$L	278	36365.6	89.100	1890	$\pi \to \pi^*$				
	355	28575.4	130.200	2130	$n \to \pi^*$				
Bipy	240	41666.6	2.432	2432	$\pi \to \pi^*$				
	285	35087.7	2.926	2926	$n \to \pi^*$				
[Cr(L)(bipy)Cl]	326	30674.8	0.748	748	$\pi \to \pi^* + n \to \pi^*$	11	3.771	d^2 sp^3	T$_2$g^3 eg^0
Octahedral	537	18621.9	0.259	259	^{4}A2g$\to^4$T1g$_{(P)}$				
	719	13908.2	0.284	284	^{4}A2g$\to^4$T1g$_{(F)}$				
	798	12531.3	0.293	293	^{4}A2g$\to^4$T2g$_{(F)}$				
[Ni(L)(bipy)H$_2$O]	291	34364.2	0.710	710	$\pi \to \pi^*$	8	2.21	sp^{3}d^2	T$_2$g^{6}eg^2
Octahedral	368	27173.9	0.947	947	$n \to \pi^* + $ C.T				
	719	13908.2	0.198	198	^{3}A1g$\to^3$T2g$_{(F)}$				
	763	13106.1	0.187	187	^{3}A1g$\to^3$T1g$_{(F)}$				
	821	12180.2	0.169	169	^{3}A2g$\to^3$T1g$_{(P)}$				
[Fe(L)(bipy)Cl]	394	25380.7	0.662	662	$\pi \to \pi^*$	13	5.69	sp^{3}d^2	T$_2$g^{3}eg^2
Octahedral	321	31152.6	0.865	865	$n \to \pi^* + $ C.T				
	617	16207.4	0.239	239	^{6}A1g$\to^4$Eg$_{(G)}$				
	634	15772.8	0.243	243	^{6}A1g$\to^4$T2g$_{(G)}$				
[Mn(L)(bipy)H$_2$O]	268	37313.4	2.594	2594	$\pi \to \pi^*$	20	5.17	sp^{3}d^2	T$_2$g^{3}eg^2
Octahedral	433	23094.6	0.141	141	^{6}A1g$\to^4$Eg$_{(G)}$				
	462	21645.0	0.134	134	^{6}A1g$\to^4$T2g$_{(G)}$				
	491	20366.5	0.126	126	^{6}A1g$\to^4$T1g$_{(G)}$				
[Co(L)(bipy)H$_2$O]	287	34843.2	1.257	1257	$\pi \to \pi^*$	18	3.88	sp^{3}d^2	T$_2$g^{6}eg^1
Octahedral	338	29585.7	1.057	1057	$n \to \pi^*$				
	617	16207.4	0.647	647	^{4}T1gF$\to^4$T1g$_{(P)}$				
	679	14727.5	0.527	527	^{4}T1gF$\to^4$A1g$_{(F)}$				

Table 4. TGA data of the complexes

Compound	Step	T$_{i/°C}$	T$_{f/°C}$	Weight mass loss (%)		Reaction
				Estimated	Calculated	
Mn-complex	1	52.37 °C	301.44 °C	22.283% experimental	22.746% theoretical	-H$_2$O-C$_6$H$_8$N
	2	307.09 °C	555.66 °C	62.757%	62.755%	-C$_{19}$H$_9$N$_4$O MnO
Calculated: 85.501%, Final = 14.499%; Estimated: 85.040%, Final = 14.960%						
Fe-complex	1	163.44 °C	239.24 °C	23.587%	23.593%	-Cl -C$_4$H$_6$NOH
	2	242.21 °C	382.71 °C	12.533%	12.726%	-C$_4$H$_3$N
	3	382.71 °C	571.41 °C	49.413%	49.536%	-C$_{17}$H$_7$N$_3$ FeO$^+$
Calculated: 77.252%, Final = 22.748%; Estimated: 71.8796%, Final = 28.1204%						
Ni-complex	1	69.46 °C	228.62 °C	16.743%	16.930%	-H$_2$O, -C$_3$H$_2$N$_2$
	2	236.84 °C	348.83 °C	16.326%	16.060%	-C$_5$H$_4$OH
	3	391.64 °C	559.75 °C	51.598%	51.806%	-C$_{17}$H$_{10}$N$_3$ NiO
Calculated: 84.854%, Final = 15.146%; Estimated: 84.609%, Final = 15.391%						

492.39

$C_{25}H_{19}N_5O_3Mn$

52.37–301.44 °C | -H₂O

22.283% experimental | -C_6H_8N
22.746% theoretical

$C_{19}H_9N_4O_2Mn$

307.09–555.66 °C | -$C_{19}H_9N_4O$

62.757% experimental
62.755% theoretical

MnO

510.73

$C_{25}H_{17}N_5O_2FeCl$

163.44–239.2 °C | -Cl

23.587% experimental | -C_4H_6NOH
23.593% theoretical

$C_{21}H_{10}N_4OFe$

242.21–382.71 °C
| -C_4H_3N
12.533% experimental
12.726% theoretical

$C_{17}H_7N_3OFe$

382.71–571.41 °C
| -$C_{17}H_7N_3$
49.413% experimental
49.536% theoretical

FeO⁺

496.14

$C_{25}H_{19}N_5O_3Ni$

69.46–228.62 °C | -H₂O

16.743% experimental | -$C_3H_2N_2$
16.930% theoretical

$C_{25}H_{15}N_3O_2Ni$

236.84–348.83 °C
| -C_5H_4OH
16.326% experimental
16.060% theoretical

$C_{17}H_{10}N_3ONi$

391.64–559.75 °C | -$C_{17}H_{10}N_3$

51.598% experimental
51.806% theoretical

NiO

Scheme 4. Suggested decomposition reaction of complexes

stage lost its equivalent weight of C_6H_8N and H₂O in a practical percentage of 22.283%, which is close to theoretical calculation. The second stage had lost equivalent weight of $C_{19}H_9N_4O$ in a practical percentage of 62.757%, which was close to that calculated theoretically. The remaining was manganese oxide, as in the curve shown in Fig. S10, where the percentage of total weight lost was 85.04%, and the remaining was 14.96%, which goes back to the remaining metal oxide [20].

The decomposition of the iron complex included three stages. The first stage had lost its equivalent weight of C_4H_6NOH and Cl in a practical percentage of 23.587%, close to that calculated theoretically. The second stage had lost equivalent weight of C_4H_3N in a practical percentage

of 12.533%, which was close to that calculated theoretically. The third stage had lost equivalent weight of $C_{17}H_7N_3$ in a practical percentage of 49.413%, which was close to that calculated theoretically. The remaining was FeO⁺, as in the curve shown in Fig. S11 where the percentage of total weight lost was 71.8796%, and the remaining was 28.1204%, which goes back to the remaining metal oxide [16]. The decomposition of the nickel complex included three stages; the first stage had lost its equivalent weight of $C_3H_2N_2$ and H₂O in a practical percentage (16.743%), close to theoretical calculation. The second stage had lost equivalent weight of C_5H_4OH in a practical percentage of 16.326%, which was close to that calculated theoretically. The third stage

Table 5. Thermal decomposition (DSC) of complexes

Compound	$T_{i/°C}$	$T_{f/°C}$	Maximum temperature point (°C)	ΔH (J/g)	ΔS (J)	ΔG (J)	Type
Mn-complex	87.65	195.13	132.40	−63.03	−0.586	14.5564	endothermic
	387.65	395.13	392.40	−3.03	−0.405	155.8920	endothermic
Fe-complex	153.16	157.31	159.33	−0.59	−0.142	22.0348	endothermic
	314.19	319.29	313.67	−3.44	−0.674	207.9730	endothermic
Ni-complex	41.08	106.52	66.81	−5045	−77.093	5.1001	endothermic
	127.85	172.88	150.79	−27.08	−0.601	63.5440	endothermic
	182.36	196.21	189.75	−1.19	−0.085	14.9380	endothermic
	218.84	305.41	254.77	238.78	−2.758	463.8700	exothermic

Table 6. Radical scavenging activities, percentage inhibition and IC_{50} values

Comp.	Concentration (mg/mL)	PI (%)	RSA (%)	IC_{50} (mg/mL)
Gallic acid	0.008	18.730	81.270	0.014
	0.004	45.690	54.310	
	0.002	60.350	39.650	
	0.001	68.160	31.840	
	0.0005	72.360	27.640	
[Cr(L)(bipy)Cl]	0.008	17.630	82.370	0.026
	0.004	34.340	65.660	
	0.002	40.420	59.580	
	0.001	33.060	66.940	
[Mn(L)(bipy)H₂O]	0.008	20.430	79.570	0.023
	0.004	46.430	53.570	
	0.002	49.330	50.670	
	0.001	40.190	59.810	
[Fe(L)(bipy)Cl]	0.008	29.090	70.910	0.020
	0.004	35.750	64.250	
	0.002	40.160	59.840	
	0.001	50.620	49.380	
[Co(L)(bipy)H₂O]	0.008	14.090	87.910	0.020
	0.004	22.750	77.250	
	0.002	36.160	63.840	
	0.001	32.620	67.380	
[Ni(L)(bipy)H₂O]	0.008	24.430	75.570	0.039
	0.004	36.820	63.180	
	0.002	38.960	61.040	
	0.001	47.620	52.380	

IC_{50}: the half maximal inhibitory concentration

back to the remaining metal oxide [20-21]. The thermodynamic parameters ΔH, ΔS, and ΔG were calculated using the DCS curve [22].

Examining Antioxidant Activity

The purpose of the assessment is to find out how efficiently antioxidants can scavenge it. Antioxidants contribute to hydrazine, a hydrogen atom, which lowers the nitrogen atoms' single electrons in DPPH. Ga was utilized to assess and compare with the antioxidant activity of mineral complexes, and the DPPH test was employed to scavenge free radicals. The equivalent volume of concentrated 0.135 mM DPPH radical solution was added to each antioxidant sample after it had been diluted with the same volume of methyl alcohol. The matching hydrazine's color changes from violet to yellow. The samples were allowed to stand at room temperature in the dark for 90 min following the addition of the DPPH solution. Next, each sample's absorbance was calculated at around 517 nm. The complexes' capacity to destroy free radicals improved with a lower IC_{50} value when compared to Ga [23-30] (Ga > [Fe(L)(bipy)Cl] > [Co(L)(bipy)H₂O] > [Mn(L)(bipy)H₂O] > [Cr(L)(bipy)Cl] > [Ni(L)(bipy)H₂O]). Table 6 illustrates the interaction of the complexes with DPPH radicals and the subsequent hydrogen donation to scavenge the radicals.

■ **CONCLUSION**

To conclude, mixed ligands reaction of H₂L and bipy was successfully performed in conjunction with salts of Cr(III), Mn(II), Fe(III), Co(II) and Ni(II). Then, metal complexes were discovered utilizing a range of analytical techniques. The formed complexes have a

had lost equivalent weight of $C_{17}H_{10}N_3$ in a practical percentage of 51.598%, which was close to that calculated theoretically. The remaining was NiO, as in the curve shown in Fig. S12 where the percentage of total weight lost was 84.609%, and the remaining was 15.391%, which goes

general formula [M(L)(bipy)X]; X = Cl or H_2O whereas the ligands behaved in a tridentate chelate form. The complexes gave different octahedral shapes and were non-electrolytes. Using DPPH as a free radical and Ga as a standard material, it was discovered that the complexes' ability to inhibit free radicals varied depending on the IC_{50} value; Ga > [Fe(L)(bipy)Cl] > [Co(L)(bipy)H_2O] > [Mn(L)(bipy)H_2O] > [Cr(L)(bipy)Cl] > [Ni(L)(bipy)H_2O]. Therefore, these complexes are potentially free radical restrictors.

■ ACKNOWLEDGMENTS

■ CONFLICT OF INTEREST

The authors have no conflict of interest.

■ AUTHOR CONTRIBUTIONS

Conceptualization, data duration, project administration, and writing—original draft, Areej Kamal Assim Aldabbagh; Formal analysis, Mawlood Khalid Mawlood; Funding achievement, Abbas Ali Salih Al-Hamdani, Mawlood Khalid Mawlood, and Areej Kamal Assim Aldabbagh; Investigation, methodology, supervision, writing-review & editing, Abbas Ali Salih Al-Hamdani and Areej Kamal Assim Aldabbagh; Each author has read and approved the manuscript's published abstract.

■ REFERENCES

[1] Hamza, I.S., Mahmmoud, W.A., Al-Hamdani, A.A., Ahmed, S.D., Allaf, A.W., and Al Zoubi, W., 2022, Synthesis, characterization, and bioactivity of several metal complexes of (4-amino-*N*-(5-methyl-isaxazol-3-yl)-benzenesulfonamide), *Inorg. Chem. Commun.*, 144, 109776.

[2] Mahdi, E.S., and Alabdali, A.J., 2023, Synthesis, characterization and anti-bacterial activity of mono and binuclear Co(II) and Cr(III) mixed-ligand complexes derived from alpha-amino acid and 1,10 phenanthroline with 1,3-diaminopropan as a apacer, *J. Polym. Compos.*, 11 (Special Issue 2), S107–S117.

[3] Saha, S., Regeni, I., and Clever, G.H., 2018, Structure relationships between bis-monodentate ligands and coordination driven self-assemblies, *Coord. Chem. Rev.*, 374, 1–14.

[4] Yang, G.W., Zhang, X., Li, G.M., Yang, J., Shen, L., Chen, D.Y., Li, Q.Y., and Zou, D.F., 2018, Photochemical property of a Ru(II) compound based on 3-(2-pyridyl)pyrazole and 2,2′-bipyridine for ablation of cancer cells, *New J. Chem.*, 42 (7), 5395–5402.

[5] Obaid, S.M.H., Sultan, J.S., and Al-Hamdani, A.A.S., 2020, Synthesis, characterization and biological efficacies from some new dinuclear metal complexes for base 3-(3,4-dihydroxy-phenyl)-2-[(2-hydroxy-3-methylperoxy-benzylidene)-amino]-2-methyl propionic acid, *Indones. J. Chem.*, 20 (6), 1311–1322.

[6] Manhee, T.Q., and Alabdali, A.J., 2024, Synthesis, characterization and anticancer activity of Ni(II), Cu(II), Pd(II) and Au(III) complexes derived from novel Mannich base, *Vietnam J. Chem.*, 62 (2), 201–210.

[7] Abass, B.F., Musa, T.M.A.D., and Aljibouri, M.N.A., 2021, Preparation and spectroscopic studies of cadmium(II), zinc(II), mercury(II) and vanadium(IV) chelates azo ligand derived from 4-methyl-7-hydroxycoumarin, *Indones. J. Chem.*, 21 (4), 912–919.

[8] Mohammed, H., 2021, Synthesis, identification, and biological study for some complexes of azo dye having theophylline, *Sci. World J.*, 2021 (1), 9943763.

[9] Abdulrazzaq, A.G., and Al-Hamdani, A.A., 2023, Ni^{2+}, Pt^{4+}, Pd^{2+}, and Mn^{2+} metal ions complexes with azo derived from quinolin-2-ol and 3-amino-*N*-(5-methylisoxazol-3-yl) benzenesulfonamide: Synthesis, characterization, thermal study, and antioxidant activity, *Baghdad Sci. J.*, 20 (6), 2207–2223.

[10] Shamran Mohammed, H., Deepak Tripathi, V., Aldin Darghouth, A., and Mothhar, T., 2019, Synthesis, characterization, DFT calculation and antimicrobial activity of Co(II) and Cu(II) complexes with azo dye, *J. Phys.: Conf. Ser.*, 1294 (5), 052051.

[11] Kadhim, A.J., and Shaalan, N., 2024, Synthesis, characterization, biological, and antioxidant activity of new metal ion complexes with Schiff base derived from 2-hydroxybenzohydrazide, *Indones. J. Chem.*, 24 (6), 1851–1860.

[12] Sudhakar, C., Saravanabhavan, M., Ramesh, K.S., Badavath, V.N., Chandrasekar, S., Babu, B., and Sekar, M., 2022, Pharmacological and quantum chemical studies of 2-aminobenzo [*d*] thiazol-3-ium 4-chlorobenzenesulphonate: Synthesis, spectral, thermal analysis and structural elucidation, *Results Chem.*, 4, 100442.

[13] Al-Zahraa SH.H, F., and Al-Hamdani, A.A.S., 2024, Synthesis, characterization, thermal studies, and antioxidant activities of azo dye[2-[(3-hydroxyphenyl)diazinyl]-1,2-benzothiazol-3(2H)-one-1,1-dioxide]and metal ion complexes, *Iraqi J. Sci.*, 65 (12), 6842–6861.

[14] Al-Daffay, R.K.H., and Al-Hamdani, A.A.S., 2023, Synthesis, characterization, and thermal analysis of a new acidicazo ligand's metal complexes, *Baghdad Sci. J.*, 20 (1), 121–133.

[15] Reda, S.M., and Al-Hamdani, A.A.S., 2022, Synthesis, characterization, thermal analysis and bioactivity of some transition metals complexes with new azo ligand, *Chem. Methodol.*, 6 (6), 475–493.

[16] Mohammed, H.S., Al-Hasan, H.A., Chaieb, Z., Zizi, Z., and Abed, H.N., 2023, Synthesis, characterization, DFT calculations and biological evaluation of azo dye ligand containing 1,3-dimethylxanthine and its Co(II), Cu(II) and Zn(II) complexes, *Bull. Chem. Soc. Ethiop.*, 37 (2), 347–356.

[17] Silverstein, R.M., Webster, X.F., and Kiemle, D.J., 2005, *Spectrometric Identification of Organic Compounds*, 7th Ed., John Wiley & Son, Inc., Hoboken, New Jersey, US.

[18] Alzamili, S.K., and Shamran, M.H., 2022, Synthesis, characterization and biological activity of azo guanine and its complexes, *Res. J. Chem. Environ.*, 26 (10), 129–141.

[19] Mandour, H.S., Abouel-Enein, S.A., Morsi, R.M.M., and Khorshed, L.A., 2021, Azo ligand as new corrosion inhibitor for copper metal: Spectral, thermal studies and electrical conductivity of its novel transition metal complexes, *J. Mol. Struct.*, 1225, 129159.

[20] Ali, R.R., and Mohammed, H.S., 2021, Biological activity and latent fingerprints detection by azo quinoline dye and its complexes, *Period. Eng. Nat. Sci.*, 9 (3), 317–329.

[21] Al Daffay, R.K.H., and Al Hamdani, A.A.S., 2022, Synthesis, characterization and thermal analysis of Cr(III), Mn(II) and Zn(II) complexes of a new acidicazo ligand, *Chem. Methodol.*, 6 (7), 507–521.

[22] Ahmadi, R.A., and Amani, S., 2012, Synthesis, spectroscopy, thermal analysis, magnetic properties and biological activity studies of Cu(II) and Co(II) complexes with Schiff base dye ligands, *Molecules*, 17 (6), 6434–6448.

[23] Ashrafuzzaman, M., Camellia, F.K., Al Mahmud, A., Pramanik, M.J., Nahar, K., and Haque, M.M., 2021, Bioactive mixed ligand metal complexes of Cu(II), Ni(II), and Zn(II) ions: Synthesis, characterization, antimicrobial and antioxidant properties, *J. Chil. Chem. Soc.*, 66 (3), 5295–5299.

[24] Mohammed, H.S., 2020, Synthesis, characterization, structure determination from powder X-ray diffraction data, and biological activity of azo dye of 3-aminopyridine and its complexes of Ni(II) and Cu(II), *Bull. Chem. Soc. Ethiop.*, 34 (3), 523–532.

[25] Abdullah, A.M., and Al-Hamdani, A.A.S., 2024, Synthesis, characterization, thermal studies and antioxidant activities of transition metal complexes with azo dye ligand, *Baghdad Sci. J.*, 21 (5), 1512–1535.

[26] Abd, S.S., Alkam, H.H., and Al-Shemary, R.K.R., 2023, Composition, depiction, antibacterial, antioxidant, and cytotoxicity activities studies of a new nano-sized binuclear metal (II) Schiff base complexes, *AIP Conf. Proc.*, 2414 (1), 050011.

[27] Saleh, T.A.K., Al-Samarrai, R.R.H., and Abdul-Razzaq, N.E., 2019, The antioxidant and antimicrobial activity for some new synthesized Schiff bases derived from ascorbic acid, *Int. J. Res. Pharm. Sci.*, 10 (2), 1510–1515.

[28] Vhanale, B., Kadam, D., and Shinde, A., 2022, Synthesis, spectral studies, antioxidant and antibacterial evaluation of aromatic nitro and halogenated tetradentate Schiff bases, *Heliyon*, 8 (6), e09650.

[29] Kareem, M.J., Al-Hamdani, A.A.S., Jirjees, V.Y., Khan, M.E., Allaf, A.W., and Al Zoubi, W., 2021, Preparation, spectroscopic study of Schiff base derived from dopamine and metal Ni(II), Pd(II), and Pt(IV) complexes, and activity determination as antioxidants, *J. Phys. Org. Chem.*, 34 (3), e4156.

[30] Mahmoodi, N.O., Ahmadi, A., Yazdani Nyaki, H., Taherpour Nahzomi, H., and Panahi Kokhdan, E., 2022, Efficient synthesis of new azo-sulfonamide derivatives and investigation of their molecular docking and cytotoxicity results, *Arabian J. Chem.*, 15 (12), 104383.